Chapter 03: Manufacturing and Characterization of Aluminium Matrix Composite

3.1 Preamble

The literature survey attempted in the previous chapter revealed that the stir casting process is the most appropriate and economical method for manufacturing composites having a uniform distribution of reinforcement particles. Thus for the present investigation, Aluminium Matrix Composites (AMC) is manufactured using the stir casting process. To understand the effect of the addition of reinforcement particles, characteristics of as-cast composites such as microstructure, mechanical and tribological properties were evaluated and compared with as-received aluminium alloy. The subsequent sections discuss the manufacturing procedure and characterization of AMC.

3.2 Manufacturing Procedure

The manufacturing of AMC was accomplished using the stir casting process. The stir casting setup consists of two components (i) the furnace and (ii) the stirrer. The electric furnace that was used for melting the matrix is shown in Figure 3.1. For the present investigation, commercially available AA 2014 grade of aluminium alloy was selected as a matrix. The rod of AA 2014 was having a diameter of 25 mm and the chemical composition of AA 2014 is represented in Table 3.1. The matrix of AA 2014 was reinforced with a different weight percent of reinforcement particles. The considered reinforcement material was Silicon Carbide (SiC) and the weight percent of SiC was 5%, 10% and 15%. The particle size of considered SiC particles was between 200-300 μm and the same has been shown in Figure 3.2.

Table 3.1 Chemical Composition of AA 2014

Elements	Si	Cu	Fe	Zn	Mg	Mn	Al
Amount (%)	0.8	4.48	0.35	0.1	0.8	0.88	92.49

Figure 3.1 Electrical furnace used for melting

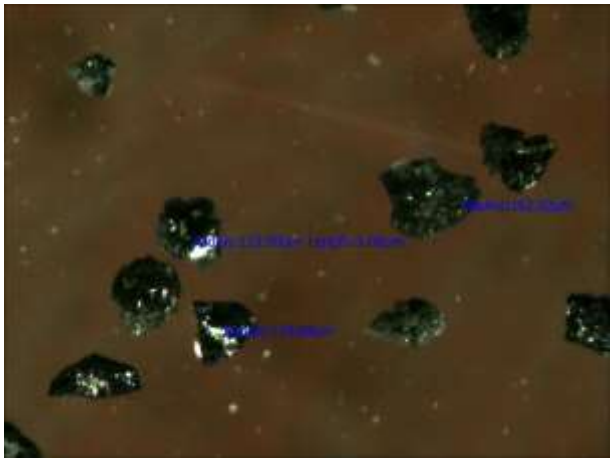

Figure 3.2 Particle size of reinforcement particle (SiC)

To fit inside the crucible, the rod of AA 2014 was cut into small lengths each of 100 mm approximately. These cut pieces of matrix material were weighted and a batch of 1 kg was formed. To manufacture AA 2014 + 5% SiC, 50 grams of SiC particles were weighted and wrapped in aluminium foil for pre-heating. The batch of aluminium matrix and corresponding reinforcement particles as per weight percent is shown in Figure 3.3. Before placing the crucible, the electric furnace was pre-heated to 165 °C and once the desired temperature was attained, the crucible consisting matrix was placed in a furnace. The matrix material of AA 2014 was heated to 780 °C, slightly higher than the melting point of the matrix. In the parallel furnace, reinforcement particles were pre-heated to 350 °C for 10 minutes. On successful melting, the molten aluminium was stir such that the formation of a vortex takes place. The pre-heated reinforcement particles were then added to the vortex formed in the molten matrix. Pre-heating of reinforcement particles helps in removing the moisture content and enhances the wettability (Ravi, Naik, & Prakash,

2015). Along with reinforcement particles, 1% of magnesium was also added to the molten matrix. Literature suggests that the addition of magnesium acts as a wetting agent and it tends to improve wettability between molten matrix and reinforcement particles (Raj & Thakur, 2016). The addition of reinforcement particles directly into a vortex of the molten matrix, and stirring the molten mixture may lead to the homogeneous distribution of reinforcement particles in molten metal. As shown in Figure 3.4, the mixture was stir for 5 minutes with a stirring speed of 300 rpm. The stirrer was having 4 blades and the angle between the two blades was 60°. On completion of stirring, the slag formed on the upper surface of the molten mixture was removed and the molten mixture was poured into the mould and the same has been shown in Figure 3.5. The solidified cast component was having a dimension of 100 × 100 × 10 mm. On solidification, the cast composite was removed from the mould. Similar procedure was followed for fabrication of AA 2014 + 10% SiC and AA 2014 + 15% SiC composite. All the fabricated composites are shown in Figure 3.6.

Figure 3.3 Aluminium alloy and wrapped SiC particles as per weight percent

Figure 3.4 Formation of a vortex due to the stirring of molten composite

Figure 3.5 Pouring of molten composite in mould

Figure 3.6 AA 2014+ x wt. % SiC Composite (x = 5, 10 and 15)

3.3 Investigation on Metallurgical, Mechanical and Tribological Properties

The present section discusses the procedure adopted for investigating metallurgical, mechanical and tribological characteristics of manufactured composites. Metallurgical characteristics such as microstructure and microhardness and mechanical properties i.e. tensile strength were investigated and critical analysis has been presented in subsequent sections. Apart from this, to investigate the tribological property, a wear test was performed. The specimens for evaluation of microstructure, mechanical and tribological

properties were taken from each composition as per the schematic shown in Figure 3.7.

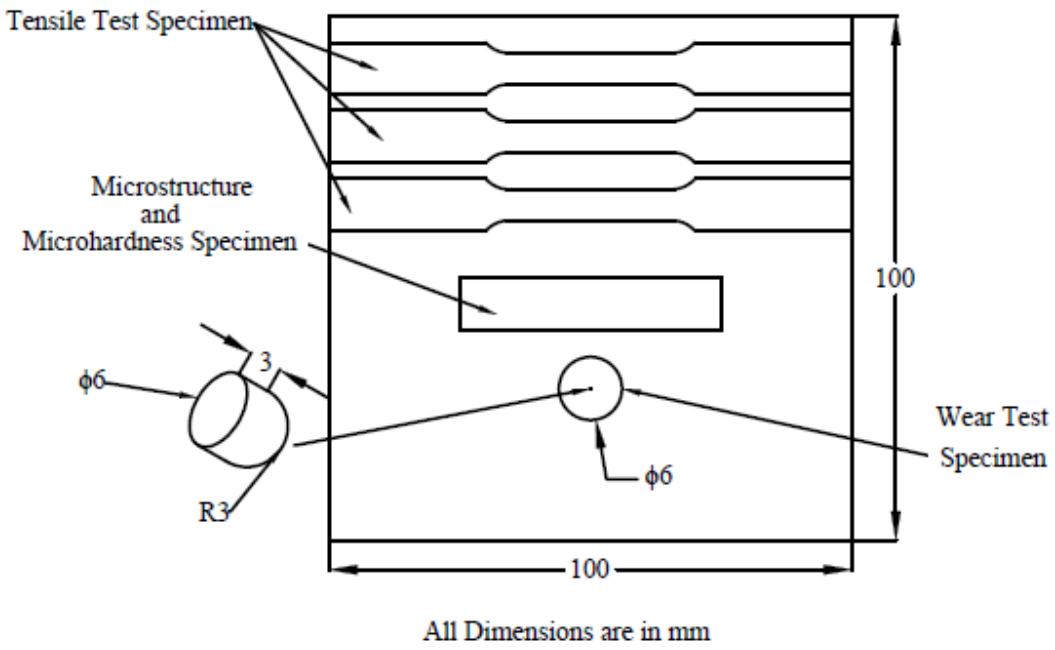

Figure 3.7 Schematic representing the specimens taken from as-cast composite for microstructure, mechanical and tribological evaluation

3.3.1 Microstructure Evaluation

Microstructural characteristics of manufactured composites were investigated using Optical Microscope (OM). The specimen required for each investigation was cut from as-cast composite as per Figure 3.7 and was polished according to the standard metallurgical procedure. For etchant, Keller's reagent was prepared by mixing distilled water, nitric acid, hydrochloric acid and hydrofluoric acid in proportionate quantity. Keller's reagent was then applied on the polished surface of the specimen at room temperature and was dried out before microstructure examination.

3.3.2 Microhardness Evaluation

For microhardness investigation, specimens were cut from manufactured composites and were polished as per the standard procedure mentioned in the above section. The test was performed for a load of 300 gf with a dwell period of 10 secs and microhardness was measured in Vicker's Hardness Number (VHN). The indentation for measuring microhardness was performed from the bottom to the top surface at the centre of the specimen. The distance between the two indentations was 0.25 mm.

3.3.3 Tensile Strength Evaluation

To understand mechanical behavior, a tensile test was conducted on manufactured AMC. The specimens for the tensile test were prepared as per ASTM E08 standards. The specimens for tensile testing were cut using wire cut Electrical Discharge Machining (EDM). The cut specimens from all composition required for tensile testing is shown in Figure 3.8. The Ultimate Tensile Strength (UTS) was measured using a computerized Universal Testing Machine (UTM). For better understanding, three specimens were taken from each composition and the average of three was considered as the final tensile strength of the composite. The dimension of the specimen for the tensile test is shown in Figure 3.9.

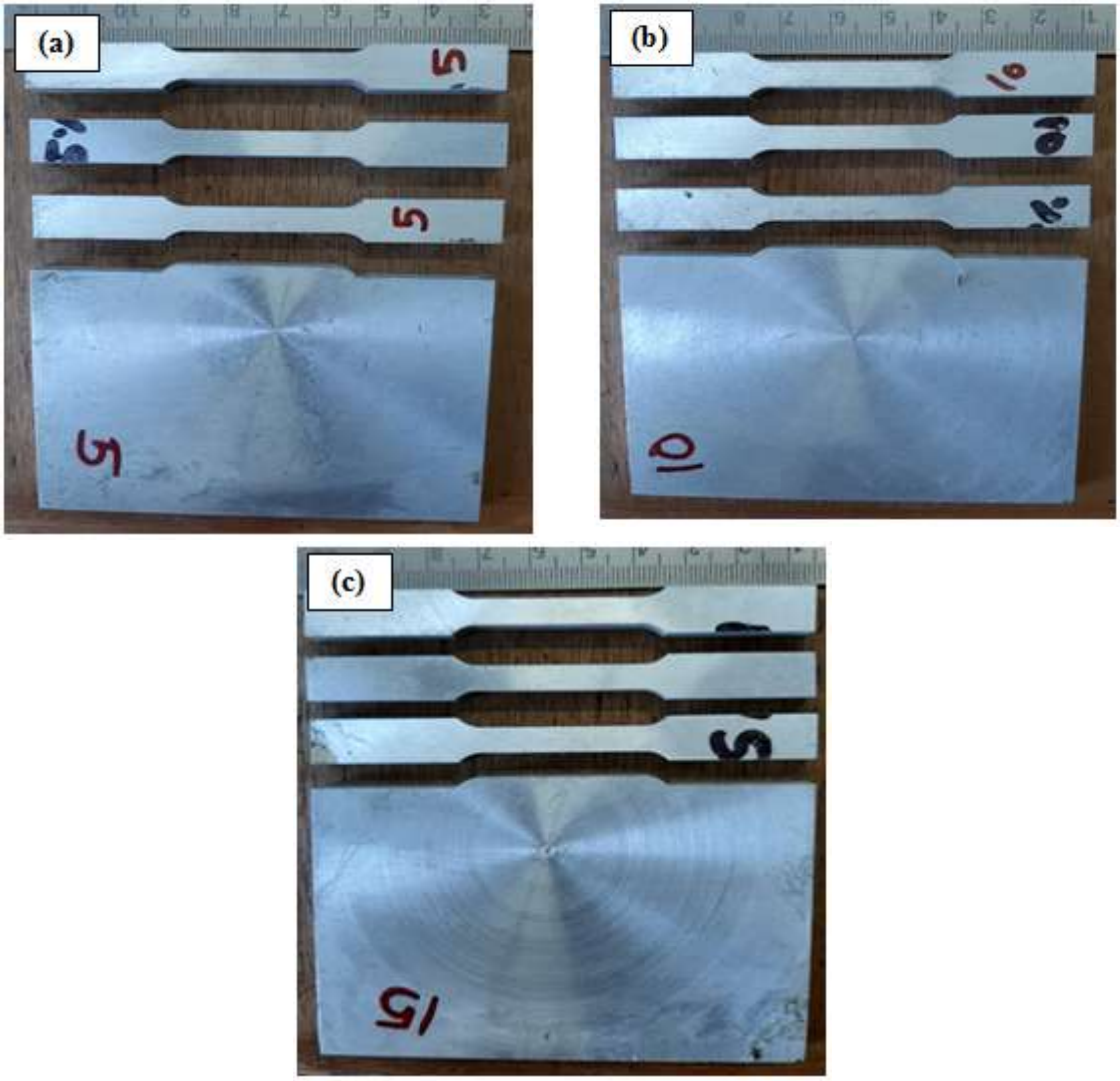

Figure 3.8 Tensile specimens cut using wire cut EDM from (a) AA 2014 + 5% SiC, (b) AA 2014 + 10% SiC and (c) AA 2014 + 15% SiC

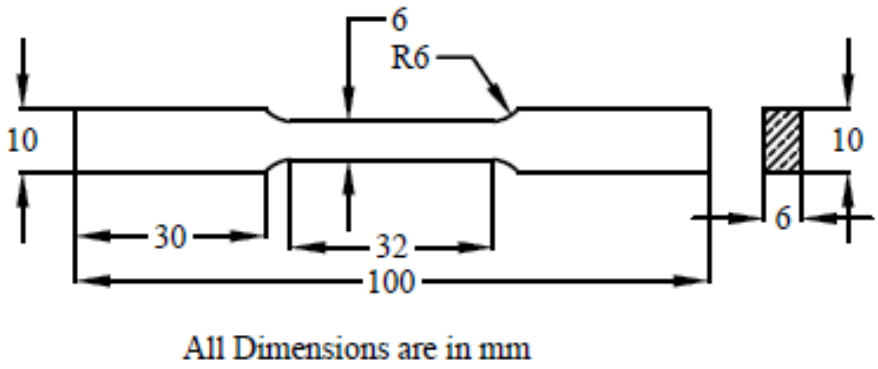

Figure 3.9 Dimension of the tensile test specimen

3.3.4 Wear Rate Evaluation

To understand the tribological characteristics of fabricated AMC, a wear test was conducted. The pin-on-disc machine that was used to perform the wear test as per ASTM standard G99-06 is shown in Figure 3.10. As per the dimension shown in Figure 3.7, the specimens required for the wear test was cut from as-cast composites using wire cut EDM. The semi-circular surface of the pin was rubbed against the EN 31 hardened steel disc of SS 304 having a hardness of 58-62 HRC. The set parameters for the wear test were: Load: 10 N, Sliding distance: 2000 m, Track diameter: 80 mm of parameters, Rotational speed of disc: 400 rpm and Sliding time: 20 min. The wear loss and coefficient of friction (COF) with respect to sliding distance were recorded and analysed.

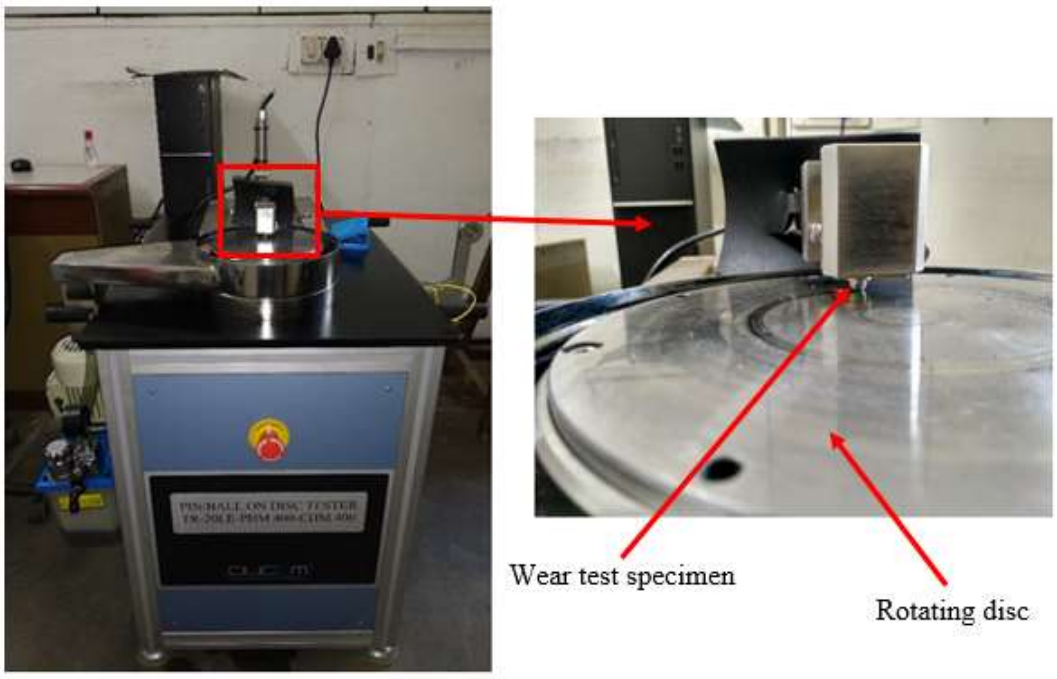

Figure 3.10 Pin-on-disc wear test machine

3.4 Result and Discussion

The subsequent section will discuss the results obtained from metallurgical, mechanical and tribological characterization.

3.4.1 Microstructure

The formation of intermetallic compounds and precipitates in aluminium alloys mainly depends upon the chemical composition of the alloy. Along with this, the condition of as-received aluminium alloy dominates the size and distribution of these phases. The microstructure of as-received AA 2014 is shown in Figure 3.12 (a). The white portions in the microstructure represent the α-Al whereas, the black portions in α-Al represents secondary phase particles. The microstructure of AA 2014 revealed finer and uniformly distributed eutectic phase in α-Al. The microstructure of as-cast composites is shown in Figure 3.11 (b) – (d). From Figure 3.11 (b) – (d), homogeneously distributed SiC particles within the α-Al matrix can be observed. Also, the increase in the weight percent of SiC particles in the matrix phase of AA 2014 can be observed from Figure 3.11 (b) – (d). It should also be noted that an increase in the weight percent of reinforcement particles doesn't alter the distribution of reinforcement particles within the matrix phase. At the same time, the increase in the weight percent of reinforcement doesn't reveal any major casting defects (apart from few voids).

The better and homogenous distribution of reinforcement particles in the aluminium matrix is attributed to the stirring action created by the stirrer. Since the entire proportion of reinforcement particles was added to the vortex formed in the molten matrix and due to the same, SiC particles are homogeneously distributed in the matrix. Owing to stirring action, reinforcement particles overcome the viscosity of the molten matrix and thus homogenous distribution of SiC particles can be observed. Also, the homogenously distributed reinforcement particles are due to the careful selection of process parameters for the stir casting process. There exist several factors which regulate the distribution of SiC particles such as stirring speed, stirring time, the viscosity of molten matrix, melting temperature, solidification rate, wettability and minimum gas entrapment (Yigezu, Jha, & Mahapatra, 2013). It should be noted that the removal of slag from the upper surface of molten composite proved beneficial towards minimization of casting defects and thus reduces the gas entrapment.

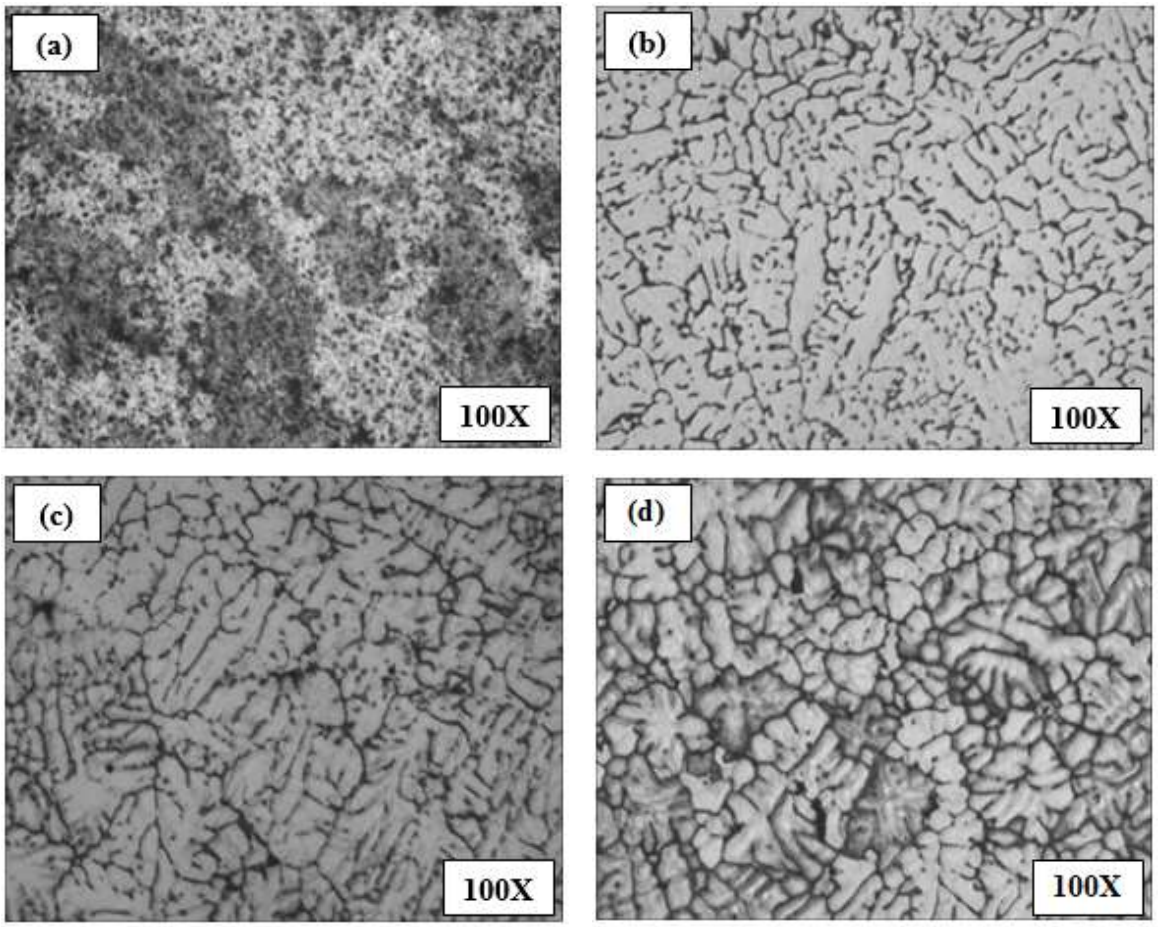

Figure 3.11 Micrograph of (a) as received AA 2014, (b) AA 2014 + 5% SiC, (c) AA 2014 + 10% SiC and (d) AA 2014 +15% SiC

At the same time, the microstructure of all manufactured composites represents proper interfacial bonding between the matrix and reinforcement phase. Pre-heating of SiC particles helps in removing impurities, desorption of gas and alters the surface composition due to the formation of an oxide layer on the surface (Hashim, Looney, & Hashmi, 2001). Apart from this, the addition of magnesium as a wetting agent has also proven beneficial for improving wettability. The addition of magnesium tends to improve the heat transfer rate and results in better contact between the composite mixture and mould interface. The wetting agent reacts with oxygen present on the surface of particles, reduces the gas layer and enhances the wettability by reducing the possibility of agglomeration (Behera, Datta, Chatterjee, & Sutradhar, 2011). Due to the combined effect of preheating of particles and the addition of wetting agents, the manufactured composites are characterized by homogenously distributed SiC with proper interfacial bonding between SiC and AA 2014.

The solidification of composites is influenced by nucleation on particles, pushing of particles due to solid/liquid interface, a chemical reaction between molten matrix and reinforcement particles and settling of particles in the molten matrix due to gravity (Ourdjini, Chew, & Khoo, 2001). While comparing Figure 3.11 (a) with Figure 3.11 (b) – (d), it can be observed that manufactured composites were found to have a dendritic like structure. This microstructure of manufactured composites was attributed to the stir casting process which leads to the formation of dendrites. From Figure 3.11 (b) – (d), it can be observed that with the increase in weight percentage of reinforcement particles, this dendritic structure tends to increase. The microstructure of AA 2014 + 15% SiC is found to have the highest dendritic formation, which was due to a higher weight percent of SiC. These dendritic structures significantly affect the mechanical properties of resulting composites (Tofigh, Rahimipour, Shabani, & Davami, 2015; Shabani, Rahimipour, Tofigh, & Davami, 2015). It is a known fact that aluminium alloys have a long freezing range. This higher cooling rate provides enough undercooling and increases nucleation sites with a reduction in dendritic arm spacing (Shabani, Baghani, Khorram, & Heydari, 2020). Thus higher cooling rate will increase nucleation with smaller nuclei. During the growth process, these small nuclei will mechanically block each other and this blocking will result in fine and uniform dendritic microstructure shown in Figure 3.11 (b) – (d). At the same time, it has been observed that reinforcement particles occupy interdendritic and secondary dendritic arm spacing. This finer spacing or finer matrix structure is the reason for the better distribution of reinforcement particles and will support towards enhancement of mechanical properties. It should be noted that the settling of reinforcement particles due to gravity results in the non-uniform distribution of reinforcement particles and thus degrades mechanical properties. Obtained microstructure doesn't evident the settling of SiC particles due to gravity in molten aluminium as SiC particles are uniformly distributed throughout the matrix.

On higher magnification, it can be observed that all the manufactured composites are characterized by the formation of the Mg_2Si phase. The presence of Mg_2Si precipitates which are formed as a thin black layer in the α-Al matrix is shown in Figure 3.12 (a). These Mg_2Si precipitates are observed in some regions inside α-Al or near grain boundaries of the α-Al matrix. Apart from this, some region of the as-cast composites was found to have a ternary eutectic phase of Al-Mg-Si. This ternary eutectic phase of Al-Mg-Si can mainly be observed at the grain boundary or junction of the Al/SiC

interface. At higher magnification, these eutectics are observed as dendrites which are generated during the final stage of solidification and precipitates of Mg_2Si can be observed as needle shape structures. It should be noted that the size of these ternary eutectics and α-Al highly depends upon mould temperature and temperature of molten mixture (Huang, Liu, Lv, Liu, & Li, 2011). As can be seen from Figure 3.12 (a), SiC particles are also observed in microstructure and are located either at grain interior or at grain boundaries. The SiC particle embedded in the α-Al matrix is shown in Figure 3.12 (b). It can also be observed that SiC particles are distributed in both transgranular and intergranular regions and good bonding between matrix and reinforcement phase can be observed. While comparing Figure 3.2 and Figure 3.12 (b), the breaking of SiC particles as a result of the stirrer can be observed. The stirrer not only helps in transferring reinforcement particles to molten metal but also tends to break these reinforcement particles into a smaller size. Due to stirring, these smaller size particles gets uniformly distributed in the molten aluminium matrix. Apart from this, the stirrer also maintains the particles in a state of suspension (Hashim, Looney, & Hashmi, 1999).

For all the manufactured composites, the average grain size of 61.95 µm was observed. This reduction in grain size indicates the breaking of SiC particles by a mechanical stirrer in the molten matrix. However, it should be noted that few locations of manufactured composites were found to have an agglomeration of SiC particles, casting defects and particles free regions. From Figure 3.13 (a), it can be observed that AA 2014 + 5% SiC composite was found to have particles free regions. Whereas, Figure 3.13 (b) AA 2014 + 10% SiC revealed the presence of few voids. Apart from this, AA 2014 + 15% SiC showed agglomeration of reinforcement particles along with a few voids at several locations. While observing Figure 3.13 (a) – (c), it can be said that increase in the weight percentage of reinforcement particles tends to avoid the formation of particles free region whereas increases agglomeration and void formation. It has been observed that due to density difference, an increase in the weight percent of reinforcement particles makes stirring difficult. Due to the same, improper stirring will take place and the travel of SiC particles within molten aluminium will be restricted. The constrained motion of SiC particles will result in the formation of agglomeration/clusters of SiC in the solidified composite. At the same time, a higher weight percent of SiC particles will increase the slag formed during the casting process. Thus, slag formation and improper stirring due to density differences may result in the formation of voids in the resulting microstructure of

composites.

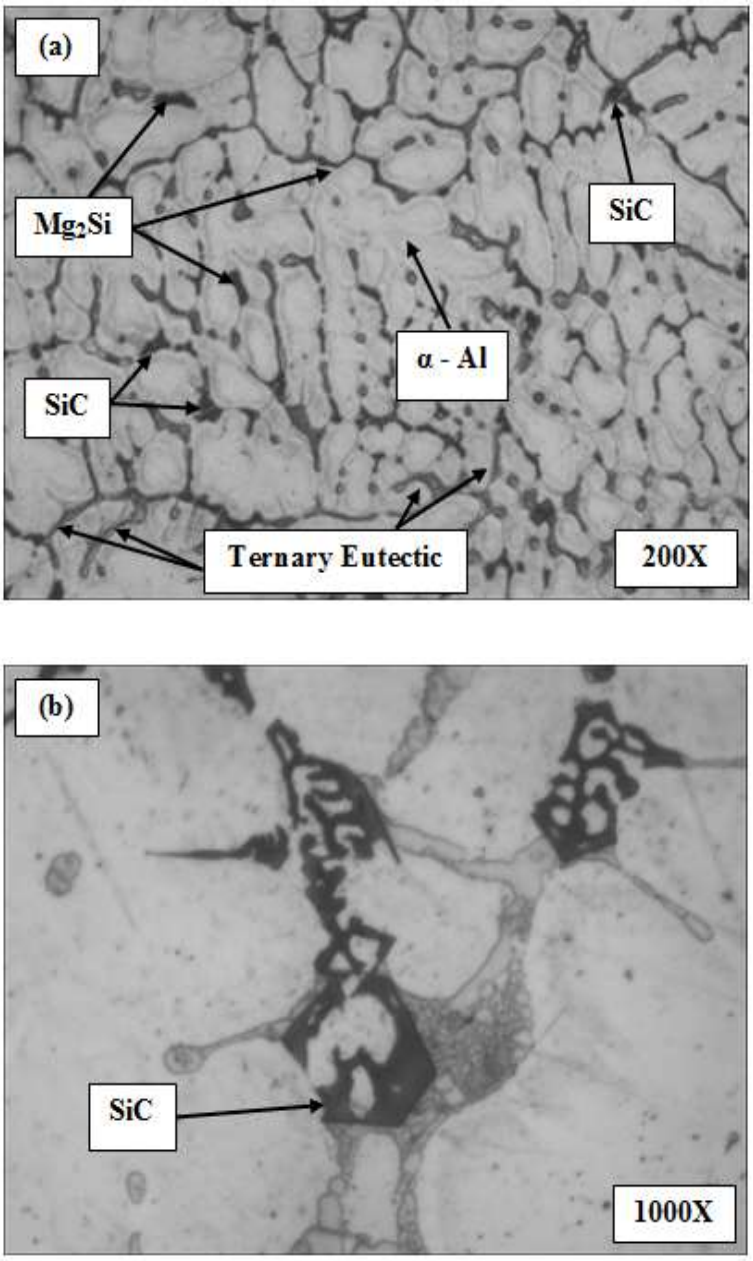

Figure 3.12 Micrograph of AA 2014 + 10% SiC (a) at 200X and (b) at 1000X

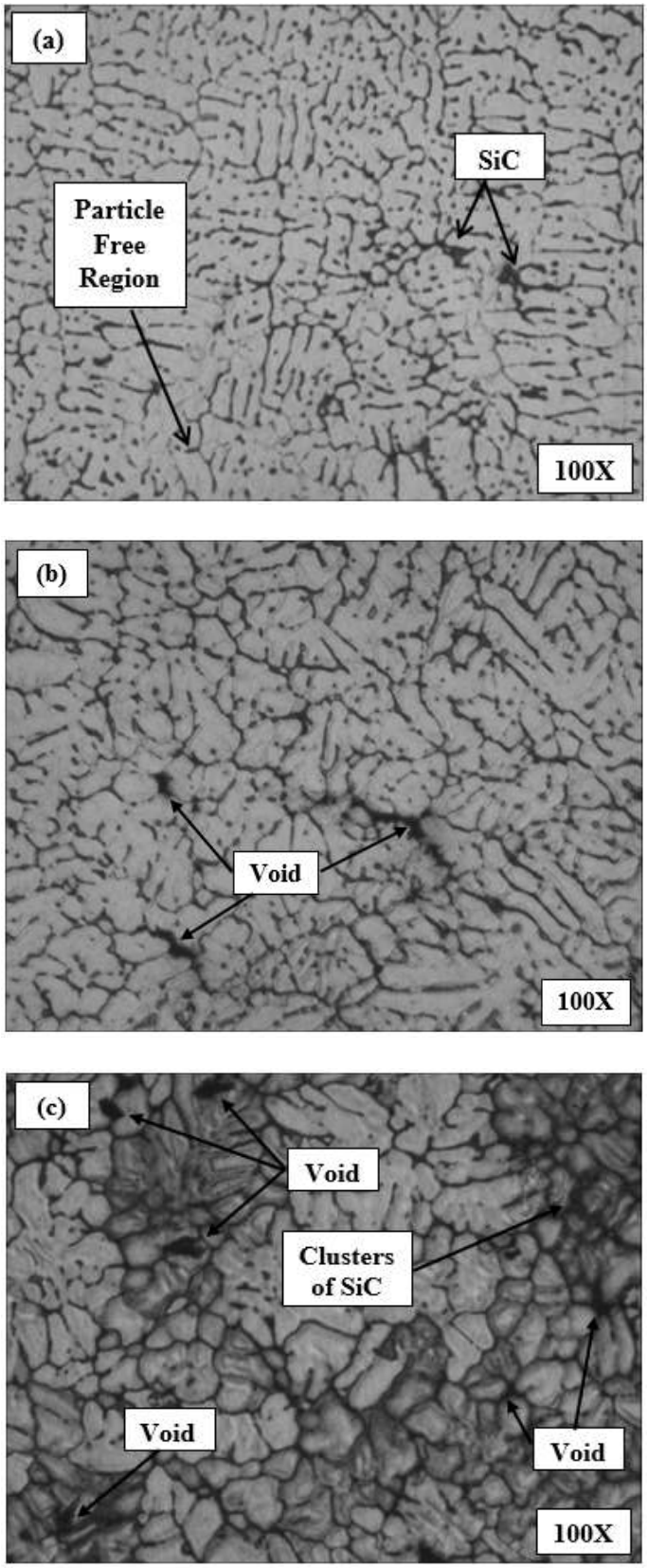

Figure 3.13 Presence of SiC clusters and particle free region in (a) AA 2014 + 5% SiC, (b) AA 2014 + 10% SiC and (c) AA 2014 + 15% SiC

3.4.2 Microhardness

As mentioned earlier, the microhardness test was conducted along the thickness of the manufactured composites. The obtained results are shown in Figure 3.14, wherein the value corresponding to zero location indicates the microhardness at the root/bottom of the specimens. It can be said that the plot of microhardness of as-received AA 2014 was almost linear without many hikes/dips. However, in Figure 3.14 there exist few sudden hikes in the microhardness of each composite. The hike in microhardness may be due to the agglomeration of SiC particles. The ceramics particles are known for their higher hardness and direct indentation on agglomeration will subsequently result in a hike of microhardness. Thus, it is possible that during measurement of microhardness, direct indentation on agglomeration was made and due to this hike in hardness was reported. Similarly, other compositions i.e. AA 2014 + 10% SiC and AA 2014 + 15% SiC also revealed presence of hikes at few locations.

Along with hikes, few dips in the plot of microhardness were also visible in as-cast composites. These dips in the plot of microhardness were attributed to particle free region. The direct indentation in particle free region will lower down the microhardness in that region. Due to the same, a sudden dip in the plot of microhardness will be evident. Apart from this, dips in the plot of microhardness can also be observed due to several casting defects such as voids and tunnels. From the plot of microhardness; it can be observed that maximum dips were reported for AA 2014 +15% SiC. This can be correlated with the results of microstructure, as AA 2014 + 15% SiC composite was found to have a higher number of microstructural defects. It should be noted that the average microhardness of all composites was higher than that of the as-received AA 2014 alloy. The average microhardness of as-received AA 2014, AA 2014 + 5%, 10% and 15% SiC were 73.45 Hv, 85 Hv, 86.76 Hv and 86.16 Hv. With the increase in weight percent of reinforcement particles from 5% to 10%, enhancement in average microhardness was reported. This enhancement in microhardness is due to the presence of a higher weight percent of SiC particles. As a result of void formation and agglomeration of SiC particles, an increase in the weight percent of SiC particles from 10% to 15% was found to have an adverse effect on average microhardness.

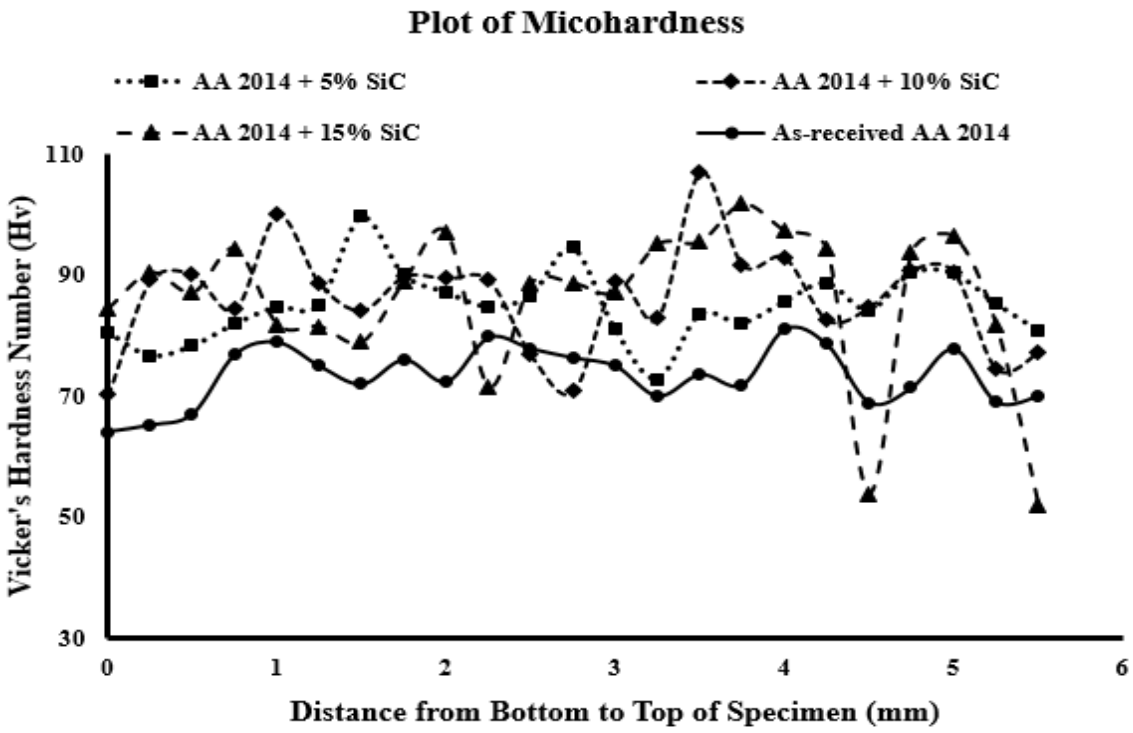

Figure 3.14 Plot of microhardness for as-cast composites

3.4.3 Tensile Strength

To investigate the tensile strength of as-cast composites, three specimens from each composition was cut using wire cut EDM as per the dimensions shown in Figure 3.9. The average of three measured tensile strengths was considered as the final tensile strength of the as-cast composite. The tensile strength of all three specimens taken from the respective composition is presented in Table 3.2. Apart from this, the graphical representation of average tensile strength is shown in Figure 3.15. From Table 3.2 and Figure 3.15, it can be observed that the as-cast composites are having higher tensile strength when compared to that of as-received AA 2014. Thus, it can be said that the addition of SiC in the matrix of AA 2014 tends to enhance the tensile strength of the resulting composites. The results revealed that Ultimate Tensile Strength (UTS) increase from 175.58 MPa for as-received AA 2014 to 225.76 MPa for AA 2014 + 10% SiC; enhancing the UTS by 28.58%. It should also be noted that with the increase in the weight percent of reinforcement particles from 5% to 10%, the UTS increases. However, with a further increase in the weight percent of reinforcement particles from 10% to 15%, the UTS was found to reduce. Overall, a 5.64% increase in UTS was observed when the weight percent of reinforcement particles increases from 5% to 10%. On the other side,

an 11.30% reduction in UTS was observed when the weight percent of reinforcement particles was increased from 10% to 15%. The observed results are in line with other results reported previously (Poovazhagan, 2013; Singh & Goyal, 2016; Singh & Chauhan, 2016). The presence of casting defects and agglomerated reinforcement particles are the possible reason for the reduction in tensile strength when the weight percent of reinforcement particles increase from 10% to 15%. It should be noted that the presence of agglomeration of SiC in AA 2014 + 15% SiC results in weaker structure/composition of the material and the presence of voids in the solidified composite will reduce the UTS of the material.

Table 3.2 Tensile strength of all specimens taken from different composition

Composition	Tensile Strength (MPa)			Average Tensile strength (MPa)	% Increase w.r.t. Base Metal	% Increase w.r.t. each composition
	1	2	3			
AA 2014	175.47	181.78	169.48	175.58	-	-
AA 2014 + 5% SiC	232.19	192.42	216.53	213.71	21.72	-
AA 2014 + 10% SiC	256.26	208.49	212.53	225.76	28.58	5.64
AA 2014 + 15% SiC	204.6	180.92	215.24	200.25	14.05	-11.30

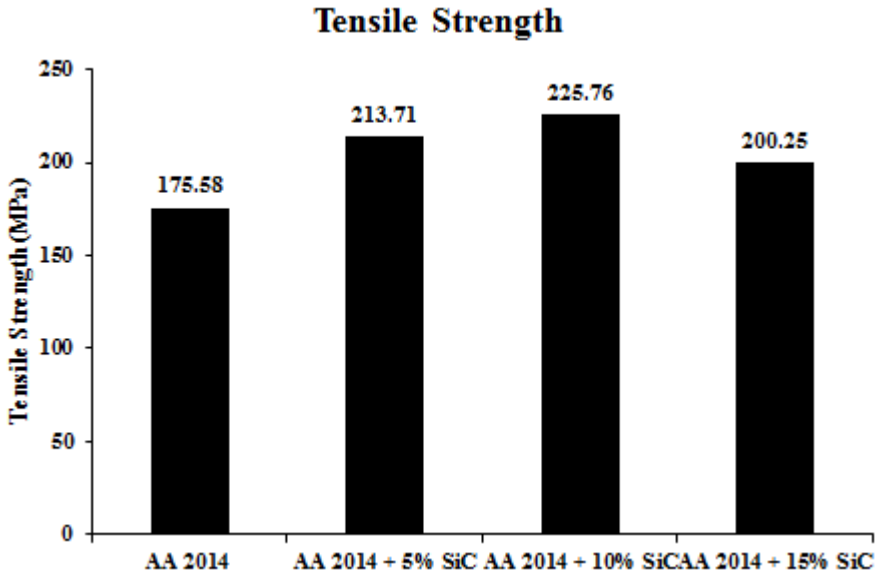

Figure 3.15 Variation in average tensile strength with increase in weight percent of SiC

Theoretical analysis suggests that enhancement in strength by addition of reinforcement particles in the matrix could be attributed to Orowan strengthening, thermal mismatch, load bearing strengthening mechanism and pinning effect of reinforcement particles (Li, et al., 2018). However, the pinning effect is more

predominant in the case of a tensile test conducted at elevated temperatures. Apart from this, the tensile strength of composites also depends upon the distribution and weight percent of reinforcement particles, concentrations of grain boundaries and dislocation densities. When compared to composites, much fewer dislocations will be generated in the aluminium alloy during solidification. Due to the absence of the pinning effect of precipitates and reinforcement particulates, the dislocation generated in the aluminium alloy can easily travel across the matrix. The motion of dislocation will restrict the mechanical properties of aluminium alloy. It should be noted that the presence of reinforcement particles and grain boundaries in as-cast composites will obstruct the dislocation motion. This obstruction will increase the hardness and strength of resulting composites (Amouri, Kazemi, Momeni, & Kazazi, 2016). A uniform distribution of finer sized reinforcement particles in the matrix is likely to generate maximum obstruction to dislocation. Thus, this will provide maximum strengthening according to Orowan strengthening mechanism (Zhang & Chen, 2008; Kim, et al., 2013). A similar observation has been reported by other researchers (Sajjadi, Ezatpour, & Beygi, 2011; Bharath, Ajawan, Nagaral, Auradi, & Kori, 2018). Another reason for the higher tensile strength of composite material is thermal mismatch strengthening. The difference in coefficient of thermal expansion, elastic modulus and shear modulus of reinforcement and matrix will promote the formation of residual stress in the vicinity of reinforcement particles. This will lead to plastic deformation during solidification and thus will enhance the density of geometrically necessary dislocation in the vicinity of the reinforcement/matrix interface. The third strengthening mechanism is load bearing strengthening mechanics. When the load is being applied on composite materials, the applied load will be transferred from ductile matrix to harder reinforcement particles. If the reinforcement particles are homogeneously distributed in the matrix, then the transfer of load will further strengthen the load bearing capacity of composites material. Thus, this will increase the tensile strength of as-cast composites (Modi 2001, Bharath, et al. 2018).

From Figure 3.16, it can be observed that all the specimens taken from as-cast composites didn't fracture at the middle of the gauge length. It should be noted that the presence of particles clusters/agglomeration or casting defects or minute impurities in as-cast composites may lead to failure from some random location. The variation in average elongation of the tensile specimen is presented in Figure 3.17. It can be observed that the average elongation of the as-cast composites is comparatively lower than that of as-

received AA 2014. Thus, it can be said that the addition of SiC particles in AA 2014 tends to reduce the elongation of the resulting composite. Apart from this, it can also be observed that average elongation reduces with the increase in the weight percent of reinforcement particles from 5% to 15%. The obvious reason for this reduction in elongation is the lower ductility of ceramic particles when compared to the ductility of AA 2014. AA 2014 + 15% SiC will have comparatively lower ductility and due to the same, the lowest elongation has been reported. With reference to as-received AA 2014 alloy, the reduction in elongation with the increase in weight percent of reinforcement particle was 42.04%, 54.49% and 61.68% respectively. Thus, it can be said that the addition of SiC particles in the AA 2014 matrix will enhance the tensile strength at an expense of a reduction in ductility.

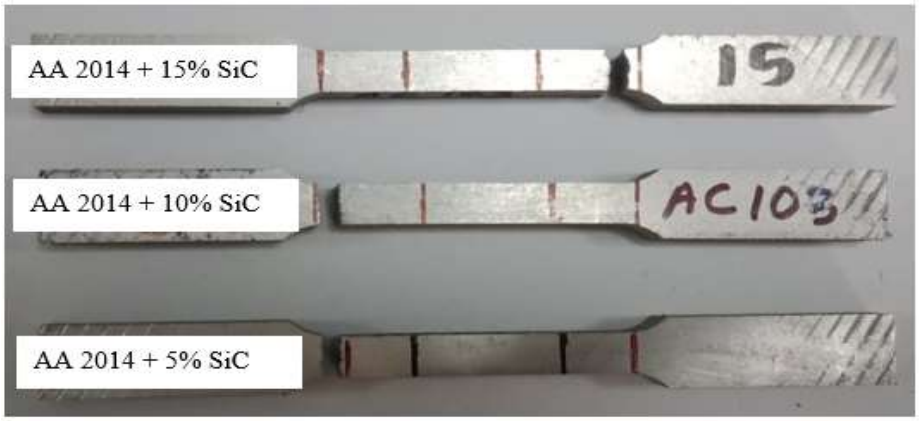

Figure 3.16 Specimens after performing a tensile test

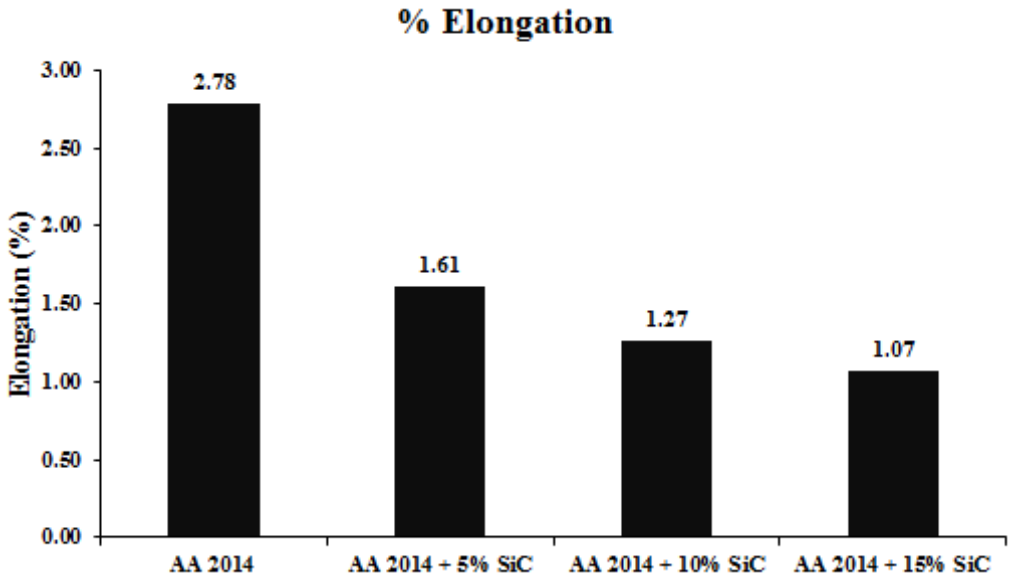

Figure 3.17 Variation in elongation with an increase in weight percent of SiC

3.4.4 Wear Behavior

The initial weight, final weight and change in weight of as-received AA 2014 and all as-cast composites are tabulated in Table 3.3. The weight of the specimens was measured using a digital weight machine having the least count of 0.001 g. The difference in change in weight was negligible for as-received AA 2014 and AA 2014 + 5% SiC composites. However, a noticeable difference in change in weight was observed for as-received AA 2014 and the other two compositions of as-cast composites. The change in weight of as-received AA 2014 was higher than that of the other two compositions of as-cast composites. From Table 3.3, it can be observed that with the increase in weight percentage of SiC particles, the difference between initial and final weight decreases.

Table 3.3 Initial weight, final weight and difference in weight of stir cast specimens

Composition	Weight before conducting wear test, W_i (g)	Weight after conducting wear test W_f (g)	Change in weight $\Delta W = W_i - W_f$ (g)
AA 2014	0.462	0.448	0.014
AA 2014 + 5% SiC	0.447	0.432	0.015
AA 2014 + 10% SiC	0.41	0.399	0.011
AA 2014 + 15% SiC	0.415	0.41	0.005

The plot of wear with respect to sliding distance for as-received AA 2014 and all as-cast composites is shown in Figure 3.18. It can be observed that the wear of both as-received AA 2014 and as-cast composites increases with the increase in sliding distance. While observing the wear plot of as-received AA 2014, a continuous increase in wear can be observed w.r.t. sliding distance. This indicates that the as-received AA 2014 doesn't offer much resistance to wear and thus wear rate increase with the increase in sliding distance. However, the wear plots of AA 2014 + 5% SiC and AA 2014 + 10% SiC composites revealed three different phases and the same are marked in Figure 3.18. Phase 1 can be identified as a phase with a maximum wear rate that took placed rapidly over a comparatively lesser sliding distance. While comparing the wear plot of AA 2014 + 5% SiC and AA 2014 + 10 % SiC composite, it can be observed that Phase 1 in AA 2014 + 10% SiC was attained within a comparatively lesser sliding distance. Apart from this, the Phase 1 of AA 2014 + 5% SiC revealed higher wear compared to AA 2014 + 10% SiC

i.e. wear in AA 2014 + 5% SiC attained comparatively higher peak in Phase 1. Data of wear test revealed that maximum wear of 432.27 microns and 364.88 microns was perceived over a sliding distance of 200 m and 140 m for AA 2014 + 5% SiC and AA 2014 + 10% SiC respectively. It should be noted that the a wear is related to asperity contact. During the initial phase, the asperities of the composite material get deformed/fractured with the progress in sliding distance. As the sliding distance progresses the contact surface of the composite material gets smoother. The contact between initial asperity on the surface of composite and rotating steel disc will increase the fluctuation in the Coefficient of Friction (COF). This increase in fluctuation will rapidly increase the wear of as-cast composites. It can be said that with the increase in sliding distance, surface morphology, effective contact area, surface roughness, surface chemistry, etc. results in the formation of Phase 1 (Wang & Rack, 1991; How & Baker, 1997; Rao & Das, 2011). In Phase 2, the wear of both composites was found to increase gradually as the sliding distance increases. From Figure 3.18 it can be observed that Phase 2 of AA 2014 + 10% SiC was comparatively longer than Phase 2 of AA 2014 + 5% SiC. Apart from this, it can be observed that the variation in wear during Phase 2 of AA 2014 +10% SiC was almost negligible. However, few nominal variations in wear can be observed during Phase 2 of AA2014 +5% SiC. By the end of Phase 1, asperities present on the surface of composites were lowered down. Due to this, a stable/gradual increase in wear of composites with the further increase in sliding distance was observed. This indeed indicates that in Phase 2, the COF has become a bit stable in comparison to Phase 1 and the wear occurs based on the surface properties such as hardness. Phase 3 can be identified as a phase in which the wear of composite material again increases. However, a rapid increase in wear (as in Phase 1) was not observed. From Figure 3.18, it can be observed that Phase 3 for AA 2014 + 5% SiC was comparatively longer than that observed in the wear plot of AA 2014 + 10% SiC. Apart from this, the AA 2014 + 5% SiC showed comparatively higher wear during Phase 3. The obvious reason for the higher wear rate of AA 2014 + 5% SiC composites is the weight percent of SiC particles. SiC particles are known for their hardness and better wear resistance. The addition of these reinforcement particles in aluminium enhances the hardness and wear resistance of the resulting composite. It should be noted that in AA 2014 + 5% SiC weight percent of SiC particles is lower and in comparison with other compositions, lower hardness was observed for AA 2014 + 5% SiC. Apart from this, microstructure investigation of AA 2014 + 5% SiC composite revealed the presence of particles free region due to lower

weight percent of SiC particles. Due to these reasons, wear and mass loss of AA 2014 + 5% SiC was comparatively higher than that of AA 2014 + 10% SiC.

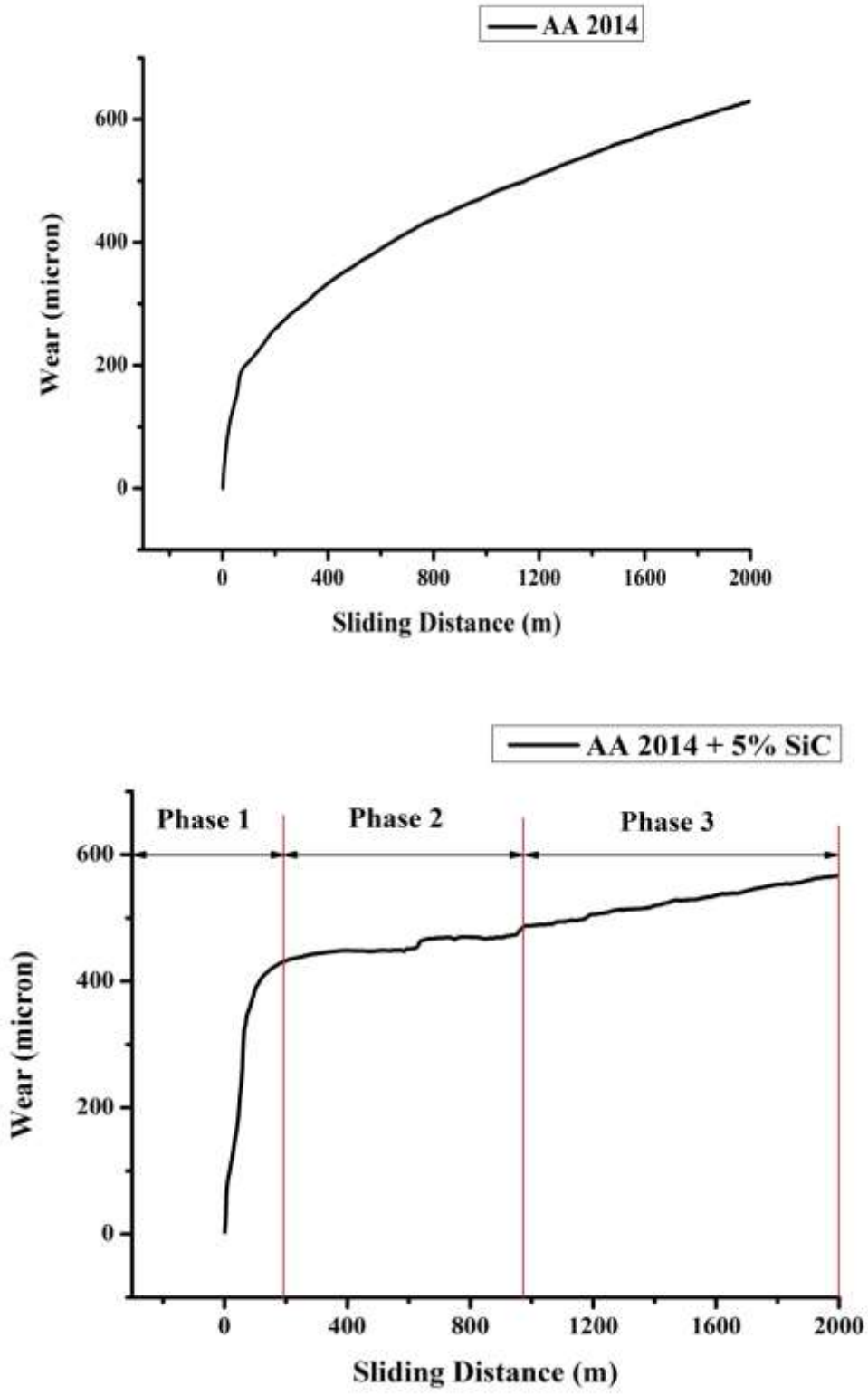

Figure 3.18 Plot of wear (microns) with respect to sliding distance (cont.)

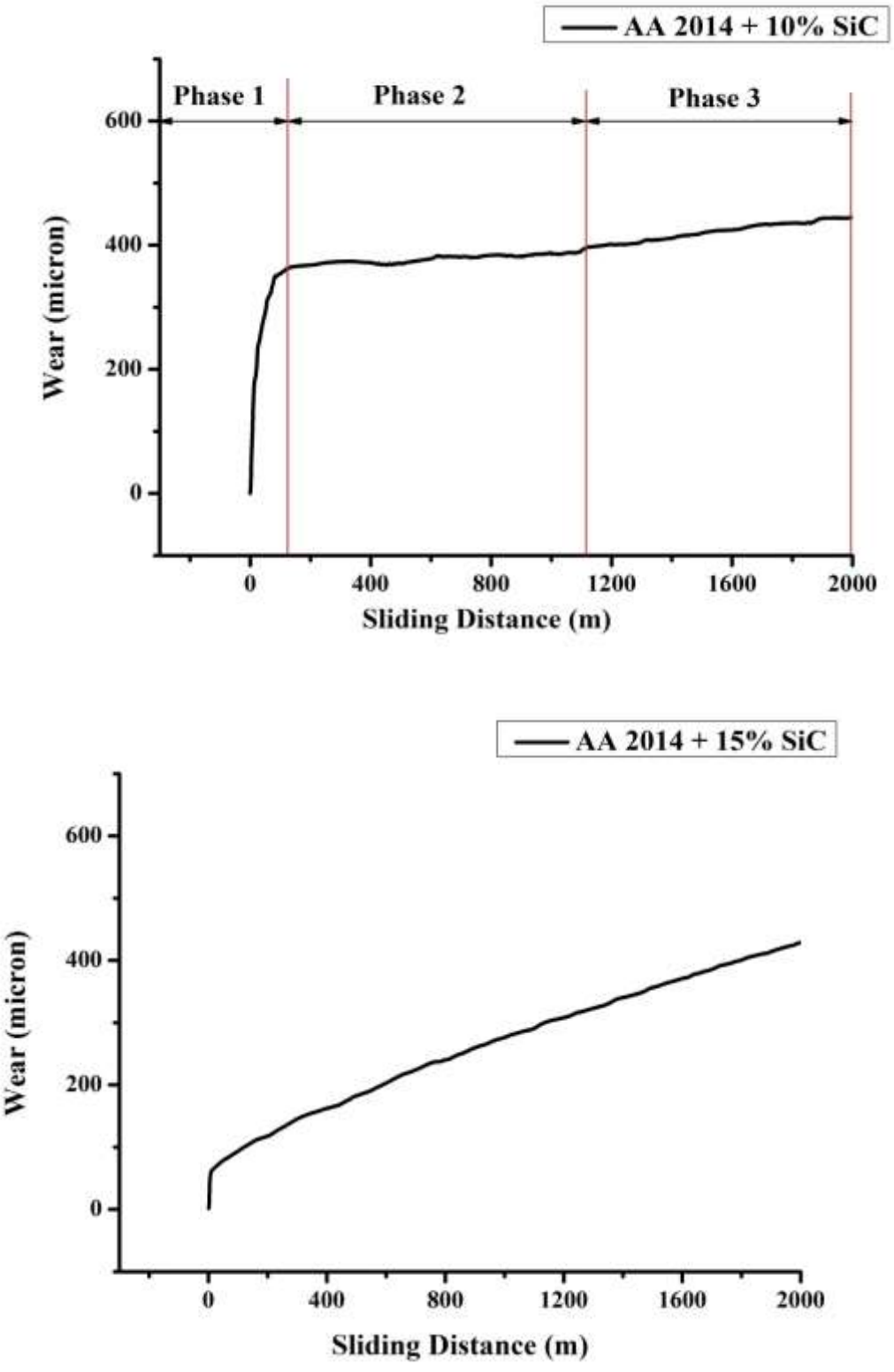

Figure 3.18 Plot of wear (microns) with respect to sliding distance

The wear plot of AA 2014 +15% SiC composites didn't reveal any phases and the same has been presented in Figure 3.18. Indeed, the wear plot of AA 2014 + 15% SiC revealed that the wear tends to increase continuously with respect to an increase in sliding

distance. One of the possible reasons for this could be surface asperities while the other could be a higher weight percent of reinforcement particles. It could be possible that due to the higher weight percent of SiC particles, the surface asperities/roughness would be more. In the case of the other two compositions, the surface asperities were resolved and the smoother surface was achieved in comparatively lesser sliding distance. Whereas, in the case of AA 2014 + 15% SiC sliding distance of 2000 m was not enough to achieve a smoother surface. Also, it should be noted that the roughness of SiC particles will tend to increase the surface asperities on wear test specimens. Thus, the continuous increase in wear with respect to sliding distance can be observed.

The plot of average wear of as-received AA 2014 and as-cast composites is shown in Figure 3.19. Except for AA 2014 + 5% SiC, other two composition revealed better wear resistance when compared to the as-received AA 2014 alloy. It should be noted that the microstructure of AA 2014 + 5% SiC composites revealed a presence particle free region and this particle free region tends to have an adverse effect on the wear resistance. Apart from this, due to the lesser content of SiC particles, the resulting composites will not provide enough wear resistance to the applied load. Thus, the highest average wear can be observed for AA 2014 + 5% composites. Lastly, it should also be noted that as-received AA 2014 was a rolled product, which tends to have comparatively lower defects. Thus, these casting defects together with lower content of SiC particles will contribute towards a higher wear rate of AA 2014 + 5 % SiC. It can be observed that with the increase in weight percent of SiC particles, the average wear of composites over a sliding distance of 2000 m reduces. The presence of SiC particles in the aluminium matrix will remarkably enhance the resulting hardness of the as-cast composite. This increase in hardness will ultimately reduce the wear rate of the composite. According to Archard law of wear, an increase in the hardness of bulk composites will increase the wear resistance of bulk composite (Archard & W., 1956; Archard J. F., 1953). Apart from this, it should be noted that the presence of SiC particles will reduce the effective contact area between the sliding pin and the rotating disc. Also, it has been reported that the normal load applied on a pin will be borne by the reinforcement particles present in the matrix and this action will reduce the coefficient of friction (Dinaharan, Saravanakumar, Kalaiselvan, & Gopalakrishnan, 2017; Xue, Xie, Xiao, Ma, & Geng, 2010; Kim H. S., 2000). Apart from supporting the load, the presence of SiC particles will also avoid the scratches and cuts caused by rotating disc and thus will enhance the wear resistance

(Zhiqiang, Di, & Guobin, 2005). An increase in weight percent of SiC particles not only increases the resistance to thermal softening but also increases the ability to support surface oxide film (Dwivedi D. K., 2003). Along with this, the presence of SiC will reduce the chances of local welding at the wear surface due to the adhesion of the wear surface with the rotating counterpart (Reddy, Bai, Murthy, & Biswas, 1994). Also, the excellent interfacial bonding between reinforcement particles and matrix will restrict/avoid the detachment of reinforcement particles from the surface of the pin. These aforementioned are the possible reasons for enhancement in wear resistance with the increase in weight percent of reinforcement particles. While comparing the wear of all as-cast composites in Figure 3.18, it can be observed that the wear plot of AA 2014 + 10% SiC was nearly a straight line (excluding Phase 1). This nominal variation in wear of AA 2014 + 10% SiC was observed due to homogenous distribution of SiC particles, lesser casting defects and absence of particle free region in the microstructure. Whereas, other two compositions i.e. AA 2014 + 5 % SiC and AA 2014 +15% SiC either revealed agglomeration of SiC or were having casting defects at the microscopic level.

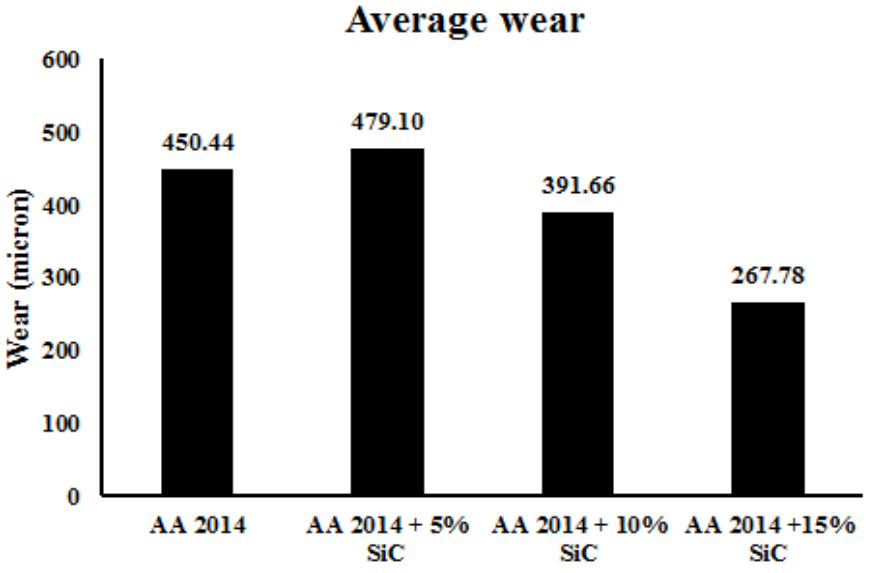

Figure 3.19 Average wear of stir cast composites

The plot of COF with respect to sliding distance is shown in Figure 3.20. For as-received AA 2014, nominal variation in COF with respect to sliding distance can be observed. As the as-received AA 2014 was a rolled product and thus it will have minimum surface asperities. Owing to this, much variations in COF was not observed. From the plot of COF of AA 2014 + 5% SiC and AA 2014 + 10% SiC, it can be observed

that initially COF rises, attains a maximum peak and then reduces over a sliding distance of approximately 300-350 m. This irregularity in COF can be observed due to surface asperities or surface roughness of the wear test specimen. The surface asperities on test specimens will act as obstacles to rotating wear disc and will result in higher opposing/frictional force against sliding. Due to the same, higher COF along with higher wear can be observed during the initial few meters of sliding distance. With the further increase in sliding distance, the surface asperities will reduce and wear will increase gradually. Owing to this, the variation in COF will reduce and thus a sideways movement in the plot of COF can be observed in Figure 3.20. For AA 2014 + 15% SiC, it was observed that initially COF increases and post attaining maximum value, negligible reduction/fall in COF was observed. The obvious reason for this could be the higher weight percent of SiC particles which are known to have comparatively higher roughness. This higher roughness will increase the frictional force during sliding friction and thus increases the COF. Among all compositions, maximum average COF was observed for AA 2014 + 15% SiC. The average COF of as-received AA 2014 was 0.31 whereas, in increasing order of weight percent of SiC particles, the average COF were 0.258, 0.267 and 0.327 respectively. It should be noted that with the increase in weight percent of reinforcement particles, wear resistance and COF of composites increase.

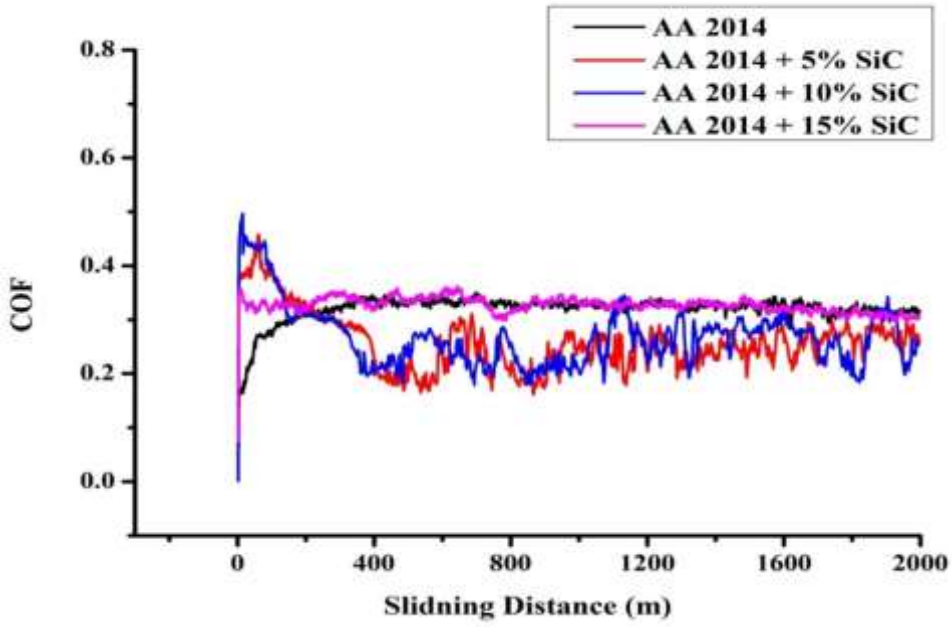

Figure 3.20 Plot of COF with respect to the sliding distance of as-received AA 2014 and as-cast composites

3.5 Summary

The present chapter demonstrates the manufacturing route i.e. stir casting adopted for manufacturing AMC. The summary of the metallurgical, mechanical and tribological properties of manufactured composites is as follows:

- Microstructure of as-received AA 2014 revealed finer and uniformly distributed eutectic phase in α-Al. When compared to as-received AA 2014, the microstructure of all as-cast composites revealed the homogeneous distribution of SiC particles within α-Al. As a result of stir casting, the microstructure of as-cast composites was found to have a dendritic structure. With the increase in weight percent of SiC particles, the dendritic in the resulting microstructure of as-cast composites was found to increase. Due to the lowest weight percent of reinforcement particles, the microstructure of as-cast AA 2014 + 5% SiC revealed particle free region. However, with the increase in weight percent these particle free regions were not observed. It should be noted that the resulting microstructure of as-cast composites was free from casting defects such as settling of reinforcement particles, the formation of deleterious phases due to chemical reaction and porosity. However, with the increase in weight percent of reinforcement particles, formation of voids was observed. Apart from this, due to the higher weight percent of reinforcement particles, the microstructure of AA 2014 +15% SiC revealed agglomeration of SiC particles. Due to stirring action generated by a mechanical stirrer, breaking of SiC particles in as-cast composites was observed. Initially, the grain size of SiC particles was 200-300 μm, which was found to reduce to 61.95 μm in as-cast composites.
- The microhardness plot of as-received AA 2014 was almost linear without many hikes/dips. Owing to the stir casting, the microhardness plot of as-cast composites revealed few hikes and dips. The presence of a hike in the plot of microhardness indicated agglomeration of SiC particles whereas, dips are observed due to casting defects. Due to the addition of SiC particles, as-cast composites revealed higher microhardness when compared to that of as-received AA 2014. The average microhardness for as-received AA 2014, AA 2014 + 5%, 10% and 15% SiC were 73.45 Hv, 85 Hv, 86.76 Hv and 86.16 Hv respectively. With the increase in weight percent of reinforcement particles from 5% to 10%, enhancement in

average microhardness was reported. Further increase in weight percent of reinforcement particles from 10% to 15% was found to have an adverse effect on microhardness.

- With respect to as-received AA 2014, all as-cast composites revealed enhancement in tensile strength. The average tensile strength of as-received AA 2014 was 175.58 MPa, which was found to increase to 213.71 MPa, 225.76 MPa and 200.25 MPa for AA 2014 + 5% SiC, AA 2014 + 10% SiC and AA 2014 + 15% SiC respectively. Similar to the microhardness, with the increase in weight percent of reinforcement particle from 5% to 10%, enhancement in tensile strength was observed. Whereas, further increase in weight percent from 10% to 15%, reduction in tensile strength was observed. Theoretical analysis suggests that enhancement in strength by addition of reinforcement particles in the matrix could be attributed to Orowan strengthening, thermal mismatch, load bearing strengthening mechanics and pinning effect of reinforcement particles. It was observed that the addition of reinforcement particles tends to reduce the elongation of resulting as-cast composites. The average elongation of as-received AA 2014 was 2.78, which was reduce to 1.61, 1.27 and 1.07 for AA 2014 + 5% SiC, AA 2014 + 10% SiC and AA 2014 + 15% SiC respectively. Thus, it can be said that the addition of SiC particles in the AA 2014 matrix will enhance the tensile strength at an expense of a reduction in ductility.
- Apart from AA 2014 + 5% SiC, the other two composites revealed enhancement in wear resistance when compared to the wear resistance of as-received AA 2014. Due to the presence of particle free region highest wear of 479.10 micron was observed for AA 2014 + 5% SiC. As-received AA 2014 revealed wear of 450.44 microns which was found to reduce to 391.66 microns and 267.78 microns for AA 2014 + 10% SiC and AA 2014 + 15% SiC respectively. With the increase in weight percent of reinforcement particles in as-cast composites, both the wear resistance and COF were found to increase. The average COF of as-received AA 2014 was 0.31 whereas, in increasing order of weight percent of SiC particles, the average COF were 0.258, 0.267 and 0.327 respectively.